

## **Classification of Large-Scale Sea-Ice Structures Based on Remote Sensing Imagery**

*Robert V. Goldstein<sup>1</sup>, Nikolai M. Osipenko<sup>1</sup> and Matti Leppäranta<sup>2</sup>*

<sup>1</sup>Institute for Problems in Mechanics, Russian Academy of Sciences, Moscow, Russia

<sup>2</sup>Department of Geophysics, University of Helsinki, Helsinki, Finland

(Received: November 1998; Accepted: October 2000)

### *Abstract*

*An analysis of satellite and aerial images of the sea-ice in the Baltic Sea was performed to trace mechanical phenomena. Characteristic structures of deformed thin-ice cover are described. Parallel faults under unidirectional tension, a concentric system of radial faults, coupled compression-tension structures, broom like shear structures, and vortex structures are discussed. A mathematical model for the formation of fault systems in unidirectional tension is presented based on fracture mechanics. Hydrodynamic resistance of the water foundation serves as the arrest mechanism for crack growth.*

*Key words: Sea ice, fracture mechanics, remote sensing, deformation*

### *1. Introduction*

On a large scale, sea-ice fields consist of a number of ice floes. The ice material in the floes appears as thermally grown sheets and, due to sea-ice mechanics, as rafted ice, rubble fields and ridges. Leads and cracks may separate the floes. The ice behaves as a continuum on a large scale, showing elastic, viscous or plastic behavior, depending on the packing density of the ice floes and loading history. As an ice continuum undergoes mechanical deformation, ordered sub-scale structures appear in the geometry, depending on the forcing and mode of deformation. These structures, identifiable in common airborne and space-borne remote sensing imagery, can be utilised to examine the life history of the ice field and for fuller understanding of the downscaling of sea-ice mechanics from the continuum length scale.

The transfer of momentum, heat and matter in the system atmosphere – sea-ice – ocean is influenced by the nonhomogeneity and structure of the ice cover. In particular, the presence of ridges or lead and crack systems has a strong influence. The formation of ordered structures can be interpreted on the basis of an analysis of the mechanics of the ice cover deformation, taking into account the influence of the loads by wind and water flow as well as the constraints created by the ice cover boundary configuration

(e.g., the harbour geometry or bay geometry). To model these structures, an approach was developed earlier (*Goldstein and Osipenko*, 1983ab, 1985, 1986, 1987, 1991, 1993; *Riska et al.*, 1996) for analysing fractures in large-scale systems, based on the determination of different scales forced by geometry and load.

In this study we have analysed aerial and satellite imagery for some mechanisms of formation of large-scale ice cover structures in the Bay of Bothnia in the northern part of the Baltic Sea. The data had been collected during 1987–1994 in several remote sensing campaigns. A classification of the structures observed was made. A series of typical structures forming ordered systems of faults in thin ice cover (ice thickness 50 cm or less) were identified. Such structures are periodic, parallel or radial cracks, echelons of faults, combined structures of faults and ridges, systems of shear faults. Examples of typical cases from the satellite images data set are given below. Finally, based on fracture mechanics a theoretical analysis is made of one structure class: the formation of fault systems in unidirectional tension.

## 2. *Mechanical phenomena in a sea-ice cover*

### 2.1 *Structural types*

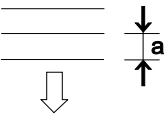
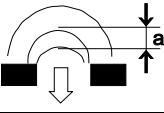
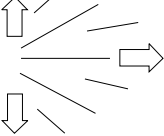
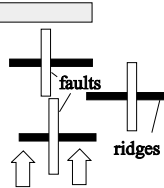
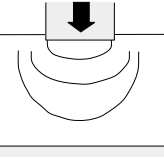
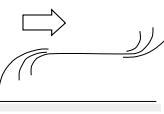
Uniform tension of ice cover causes formation of regular unloading structures of crack-like faults, which grow in a quasistatic regime in conditions close to the critical crack equilibrium in a thin viscoelastic plate. Such faults of finite length can also form an echelon-like system. Under unidirectional compressive stresses, another type of structure arises. This structure consists of a periodic system of ridges coupled with faults intersecting the ridges. Such a cross-like element of the structure (a ridge intersected by a fault) was studied earlier on model materials (*Goldstein and Osipenko*, 1987; 1991). The structural type of an ice cover fracture is strongly influenced by conditions in the water beneath the ice.

Table 1 summarises the results of the analysis performed and provides a useful interpretation tool for examining remote sensing images over sea-ice fields. The classified structures represent regular or quasiperiodic systems of faults and/or nonhomogeneities. The structures (systems of faults) resulting from free or constrained expansion can be considered as the structures of the first type. The coupled systems of ridges and faults occurring under uniform compression, as well as “broom”-like shear structures, belong to the second type. The structures tracing the water flow under ice form a special group; and their formation mechanisms are not clear. Characteristic examples of large-scale structures (Table 1) are presented in the next section.

Some problems appear when attempting to develop specific mathematical models for the formation of ice cover structures and to clarify their influence on the exchange processes which connect regional and local phenomena. The main problem is associated with the insufficiency of data concerning the details of the geometry of the struc-

tures (and their elements) and the sequence of events accompanying the ice-cover transformations in the adjacent scales. For instance, a single fault in a system of parallel faults (Table 1) can be modelled as an elongated crack-like defect, or as a system of faults of a smaller scale such they can be considered as one. These problems are also associated with other types of structures under consideration, in particular the coupled structures of compression-tension.

Table 1. Variant of the classification of the large-scale structures of the ice cover in the Bothnian Bay.

Action type	Boundary condition	Type of the structure	Structure scale (km <sup>2</sup> )	Region of probable occurrence
1. Uniform uniaxial tension caused by wind	Free boundaries	 System of parallel faults $a \sim \text{const.}$	$\sim 10^4$	Central Bay regions
	Displacement restrictions at the region boundary	 Arc-shaped faults $a \sim \text{const.}$	$\sim 10^3$	Shore regions, islands of North part of the Bay
2. Bi-axial tension caused by wind	Free boundaries	 Concentric system of radial faults	$\sim 10^4$	Region adjusting the central part of the Bay
3. Uniform compression caused by wind	Displacement restrictions in the compression direction	 System of conjugated structures of compression-tension ridges (rafts) faults	$\sim 10^4$	Region near the West Bank of the Bay
4. Local compression under motion of large mass or ice push on an obstacle	Displacement restrictions in the compression direction	 Arc-shaped structures of ridges	$\sim 10^2$	The North region of the Bay
5. Local shear caused by wind	Displacement restrictions at the fast ice boundary	 Shear with feathering "Broom" type structure	$\sim 10^3$	East and North-East regions of the Bay
6. Tracing of flows		 Rotational structures of faults and ridging regions related to the structure of underice flows	$\sim 10^4$	East and North regions of the Bay

These difficulties in classification could be overcome by performing synchronous observations of the evolution of structural elements at the appropriate adjacent scales, and by modelling the conceivable variants of the ice cover structure formation. The different mechanisms and types, which control the ice-cover reaction (deformation and fracture), are taken into account. Field studies on the localized structural elements (e.g.,

cracks, ridges) should include detailed observations of the geometry of the end regions of these elements, and of the homogeneity of the displacements in the central zones of the elements. These geometric observations should be combined with measurements of the loading characteristics.

## 2.2 Observations

We have performed an analysis of ice cover structures based on satellite and aerial images of the ice pack in the Bay of Bothnia. The data were collected during 1987–1994 on several remote sensing campaigns: BEPERS (Bothnian Experiment in Preparation for ERS-1) in 1987 (1 week) and 1988 (2 weeks) (*Leppäranta et al.*, 1992; *Askne et al.*, 1992), and BEERS (Baltic Experiment for ERS-1) in 1992, 1993 and 1994 for 1 month each year (*Leppäranta et al.*, 1993; *Carlström*, 1993; *Ulander*, 1994). The volume of data includes about 200 ERS-1 SAR images, 20 spaceborne optical images, and 30 airborne optical and radar images. The campaign observations and the weather stations of the Finnish Meteorological Institute were available for the atmospheric forcing data, providing excellent background information for the loading and ice history.

The classification of structures was made on the basis of the whole data set. The cases occurred in homogeneous ice cover of thickness 10–70 cm under the action of natural loads, which can be assumed to be uniform on the scale of characteristic structural elements. Five cases are shown below; the ice conditions and wind data were known quite well and were based on routine ice and weather data from the Finnish Institute of Marine Research and the Finnish Meteorological Institute and more detailed field observations.

### Case 1

The data are from the BEERS-92 campaign, which is reported by *Lensu* (1992). Fig. 1 shows a regular system of parallel faults associated with the stress state close to uniform unidirectional tension of ice cover. The fractures are bright in this image, probably due to the presence of surface waves. The wavelength of ERS-1 SAR is 5 cm and, therefore, only very small waves, which sometimes occur in the fractures, produce a high backscatter on the radar.

### Case 2

From BEERS-93 (*Carlström*, 1993). A concentric system of radial faults occurring under the action of biaxial tension of ice cover (Fig. 2), according to the studies performed in the central region of the basin (3 January 1993). A branching system of faults can be distinguished. The axes of the fault echelons are oriented along the wind direction determined by the centre of increased pressure (left of Fig. 2). The process of echelon formation is adjusted by using the tensile deformation in a tangential direction. In this case, the wind flows in different directions; recall that the uniaxial tension caused by the wind leads to the faults being oriented transverse to the wind direction.

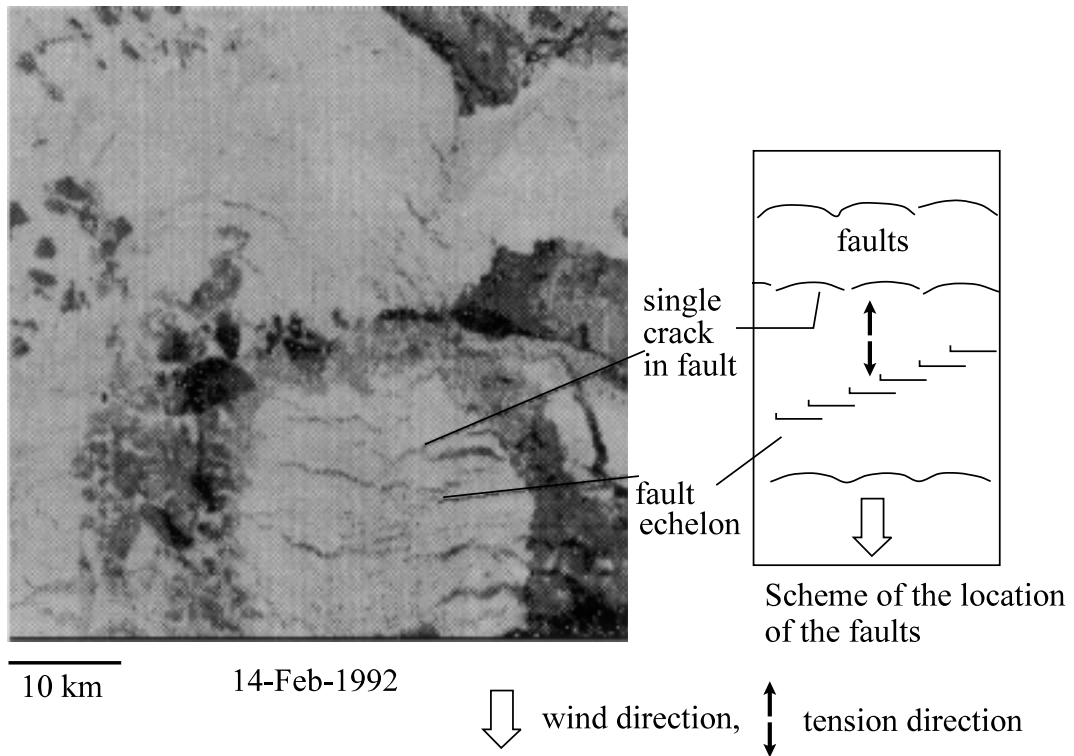


Fig. 1. ERS-1 SAR image of a system of parallel faults. © ESA

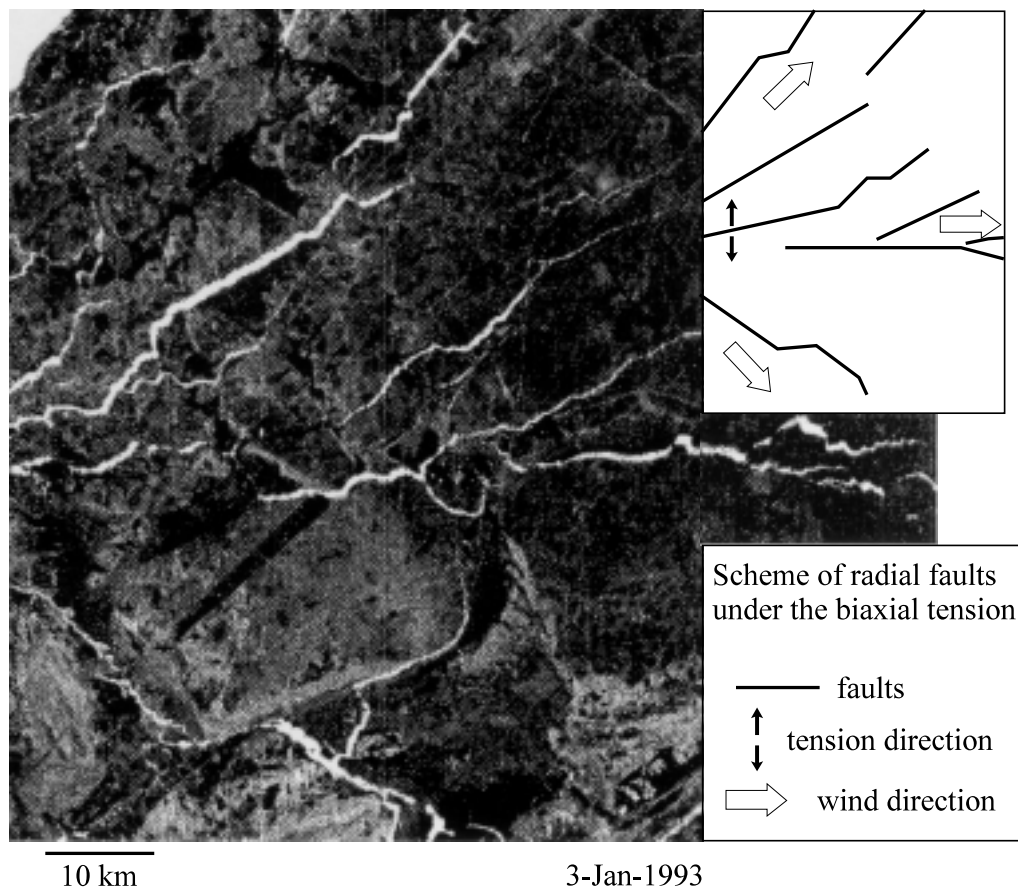


Fig. 2. A subscene of an ERS-1 SAR image of concentric system of radial faults. © ESA

Case 3

From BEERS-94 (*Ulander, 1994*). An example of a coupled structure of compression and tension (Fig. 3) in accordance with the observations performed in the northwest of the Bay of Bothnia (19 January, 1994). A characteristic cell comprises a conjugated ridge-faults structure or a conjugated rafted ice-faults structure. The ridges are oriented transverse to the wind direction, and the fault orientation coincides with the compression axis. Formation of similar structures has been observed in the laboratory testing of thin metal plates with crack-like defects under compression (*Goldstein and Osipenko, 1987; 1991*).

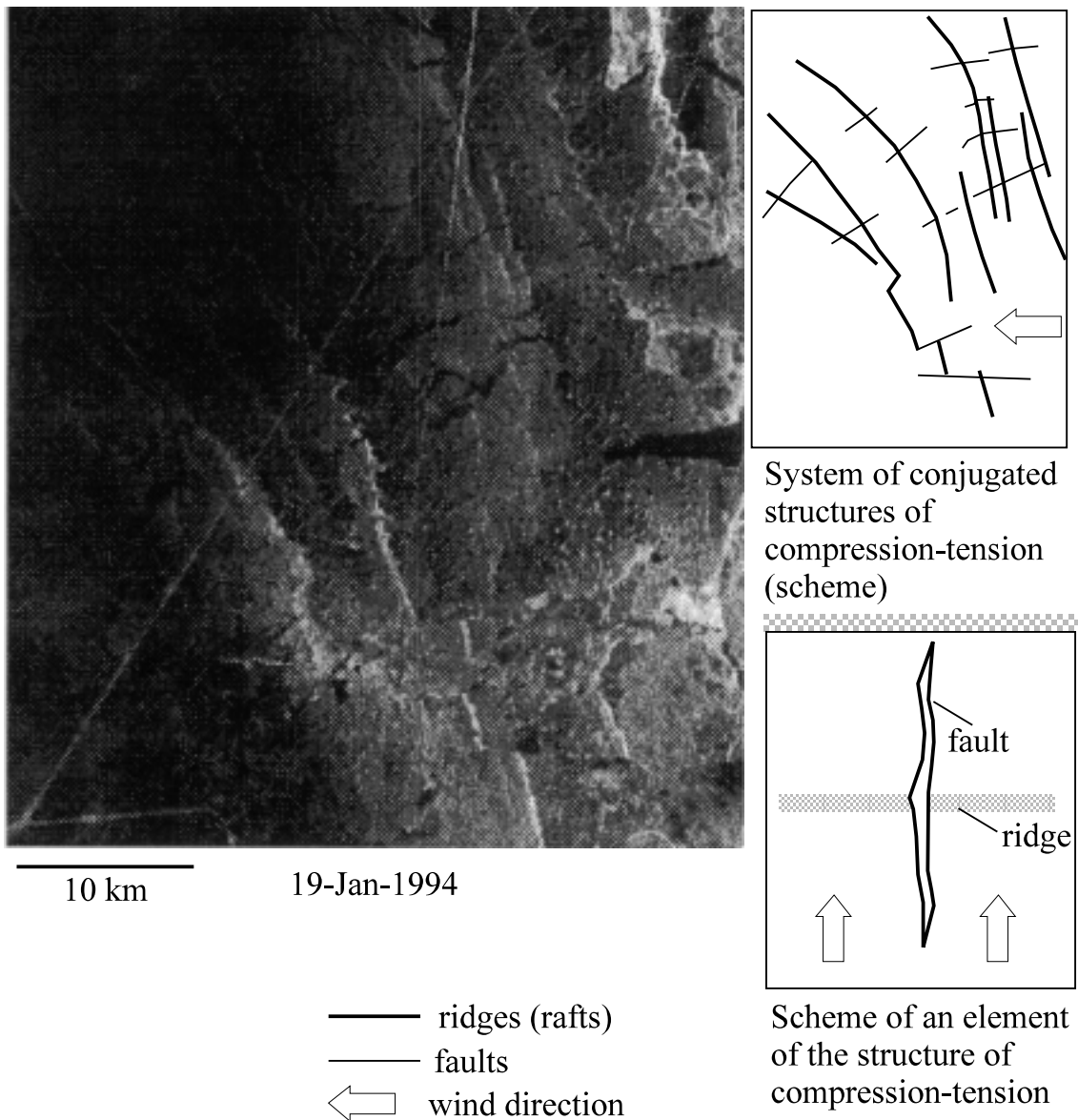


Fig. 3. ERS-1 SAR image of system of conjugated ridge – faults structures. © ESA

Case 4

From BEERS-93 (26 March, 1993). A fragment of a broom like shear structure (Fig. 4) was formed as a typical feathering of a main shear fault. Details of such a large-scale structure formation need to be clarified. One of the possible variants of its occurrence implies sequential formation of the broom branches, which consist of crack and ridge zones alternating along the main shear fault. Another possible variant is associated with the energy-conditioned kinematics of an ice field adjoining a moving shear fault. The broom-like structures are mainly observed near the fast ice boundary.

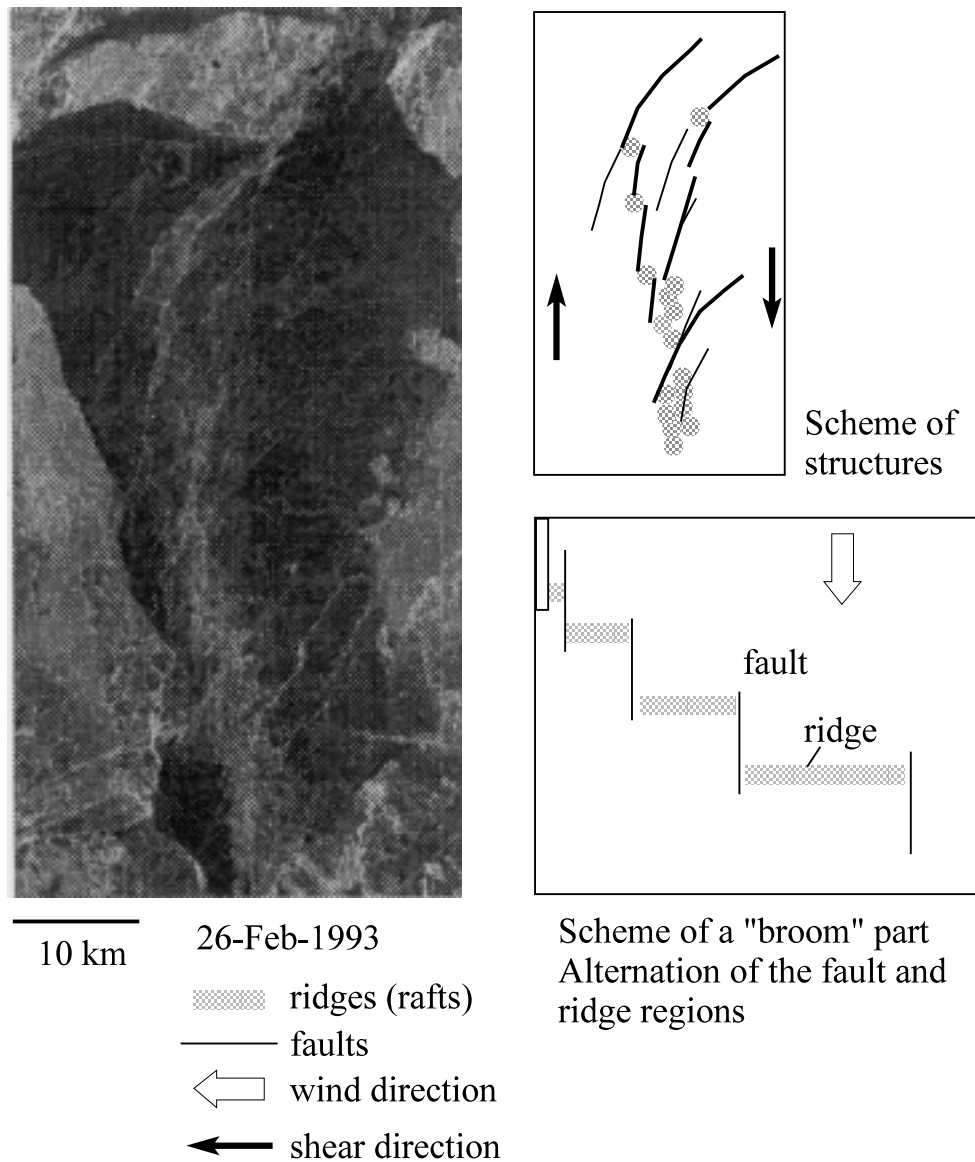


Fig. 4. ERS-1 SAR image of system of "broom" type structure. © ESA

## Case 5

From BEPERS-87 (Bothnian Experiment in Preparation for ERS-1), which is described by *Leppäranta et al.* (1992). Vortex type structures are shown in a SPOT satellite image (Fig. 5). Perhaps, these structures are a trace of a sea current beneath the ice. The main direction of the currents in the region of observations is marked by the arrow (*Zhang and Leppäranta, 1995*). The separated elements in thin ice cover (20–40 cm) have the appearance of the elements of a vortex flow associated with the general current direction. An interpretation of this structure seems to be useful both for prediction of the ice-cover state and for direct visualisation of the structure of the currents.

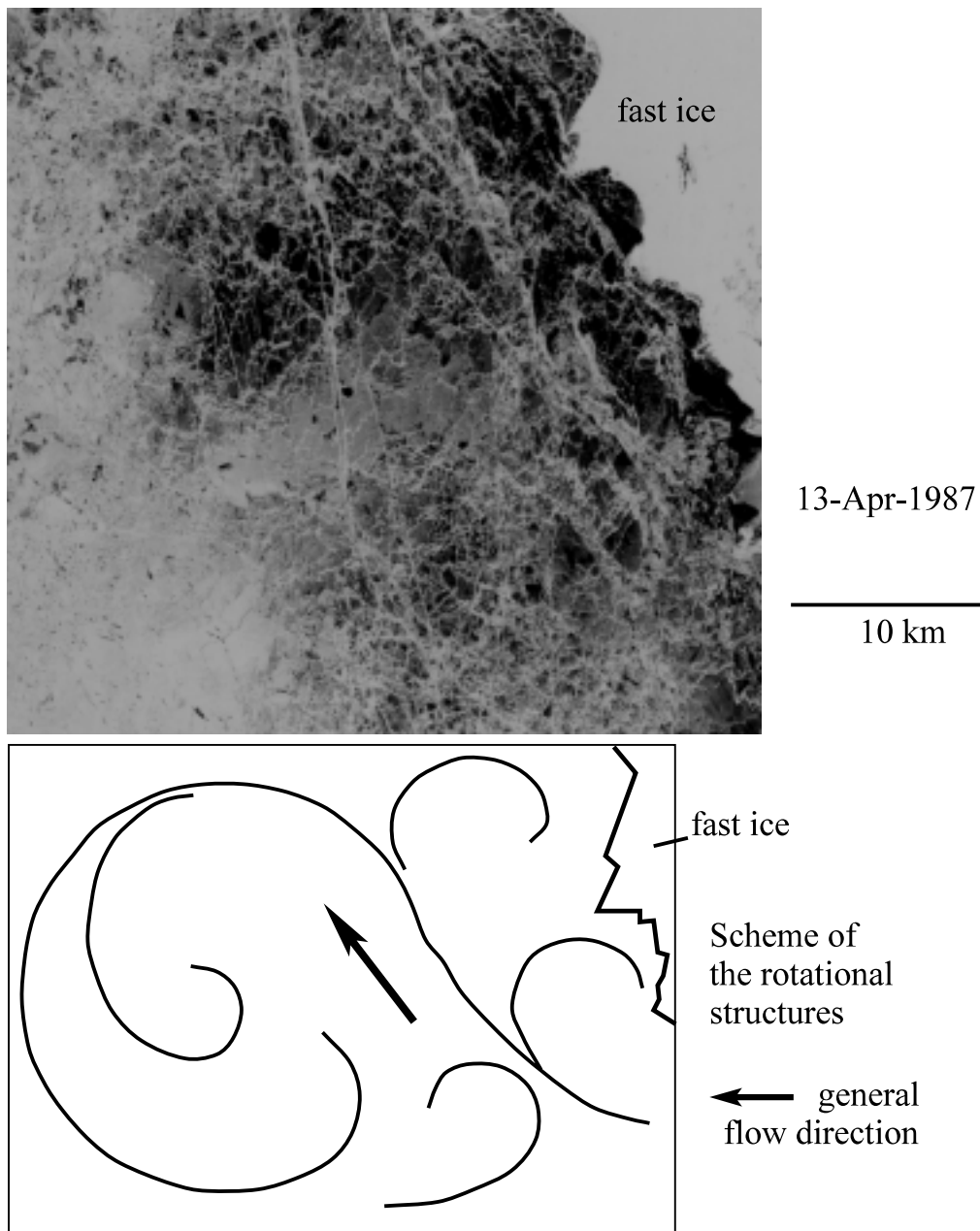


Fig. 5. Part of a panchromatic SPOT image of rotational structures (*Leppäranta et al., 1992*). Source: Satellitbild i Kiruna AB, Sweden.

### 3. Formation of fault systems

Theoretical modelling of the observed sea-ice structures has been initiated, and the first model for Case 1, the crack formation under uniaxial tension, has been completed (Type 1, Table 1). The ice cover is taken as a thin continuous viscoelastic medium.

Let us assume that the formation of a regular system of faults is caused by wind action which provides uniform tension of an initially continuous ice cover in the north-south direction. In particular, such an action can be produced if a gradient exists at the wind velocity in this direction. This assumption is indirectly confirmed by the observed 2–3 times increase of the wind velocity during the period of the fault system formation. The morphology of unitary faults and their orientation along the direction transverse to the loading axis enable us to model the faults as Type 1 cracks.

The formation of a periodic fault system under uniform tension of a continuum is a rather unusual phenomenon from the point of view of fracture mechanics. Indeed, according to the Griffith criterion, crack growth is unstable under the action of uniform tension (Hellan, 1986). However, the formation of a crack system is associated with the existence of a mechanism of crack arrest in the medium under consideration.

In Case 1, the mechanism of the crack arrest can be provided by the foundation reaction. The observations given in chapter 2 show very substantial (100–200 m) displacements of the surfaces of the faults, which are 3–4 km long. Accumulation of these displacements during the period of fault system formation (less than 24 h) can cause an essential hydrodynamic reaction. This reaction is assumed to be one of the possible reasons for the fault arrest.

Let us estimate how the water foundation influences the ice. The shear load on a rigid plate  $\tau_i$  under a translational motion can be written as follows

$$\tau_i \approx \tau_a - \rho_w c_w v^2 - \eta_w v - c \rho_i h \frac{dv}{dt} \quad (1)$$

where  $\tau_a$  is the wind stress,  $\rho_w$  is the water density,  $c_w$  is the drag coefficient in water,  $v$  is the plate velocity relative to water,  $\eta_w$  is the water viscosity,  $c$  is the coefficient of the added mass,  $\rho_i$  is the ice density,  $h$  is the ice thickness, and  $t$  is time. According to this formula, the wind load is reduced by the drag due to the relative motion between water and ice, viscous drag and inertia.

We define a critical velocity  $v^*$  such that at  $v = v^*$  the wind load is completely compensated by the hydraulic foundation resistance and, hence,  $\tau_i(v^*) = 0$  (known as the free drift condition). Neglecting the viscous drag, we obtain from Eq. (1)

$$\tau_a = \rho_w c_w v^{*2} + c \rho_i h \frac{dv^*}{dt} \quad (2)$$

The value of the wind load is related to the wind velocity,  $v_a$ , by  $\tau_a = \rho_a c_a v_a^{*2}$  where  $\rho_a$  is the air density ( $\rho_a \approx 1.3 \text{ kg/m}^3$ ), and  $c_a$  is the drag coefficient. A representative value for

the Baltic ice cover is  $ca \approx 1.8 \cdot 10^{-3}$  (Leppäranta and Omstedt, 1990). Furthermore, the average wind-induced stress  $\langle \sigma \rangle$  in an ice cover with a system of faults can be estimated similarly as in the method usually used when the fracture of brittle coatings is analysed. Then

$$\langle \sigma \rangle \sim \tau_a \Delta / h \quad (3)$$

where  $\Delta$  is the distance between the adjacent faults. This formula can be used to estimate the mean tensile strength.

Using the initial condition  $v^* = 0$  at  $t = 0$  we obtain the solution for Eq. (2)

$$v^* = \frac{\tau_a}{\rho_w c_w} \cdot \tanh \left( \frac{\sqrt{\rho_w c_w \tau_a}}{c \rho_i h} t \right) \quad (4)$$

Asymptotically, at large  $t$ , Eq. (4) is simplified into  $v^* = (\tau_a / \rho_w c_w)^{1/2}$ , which is the free drift solution (e.g., Leppäranta, 1998). By incorporating the value of the drag coefficient  $c_w \approx 3.5 \times 10^{-3}$  (Leppäranta and Omstedt, 1990), we see that the asymptotic relation for the critical velocity  $v^*$  can be used at  $t \geq 1$  h and  $v^* \approx 0.01$ – $0.30$  m/s. We can expect significant influence of the hydrodynamic effects at least for the thin ice cover, since this value of the critical velocity is close to the drift velocity. Taking into account the assumed mechanism of the wind load compensation, we can expect that the regime of the extensive fault spreading is influenced by the compensating hydrodynamic drag.

Let us model the growth of an extensive fault in the thin-ice cover as the quasistatic growth of a crack in a viscoelastic medium, more precisely the Maxwell body. The asymptotic of the normal displacements in the active end region of an extensive fault can be written in the following form:

$$u_v \sim u_e \cdot \frac{E}{\eta} \cdot t \quad (5)$$

$$u_e \sim \frac{K_I \sqrt{x}}{E} \quad (6)$$

where  $u_v$  and  $u_e$  are the normal displacements of the fault surfaces in viscous and elastic medium, respectively,  $x$  is the distance from the fault tip along the fault,  $E$  is the Young modulus of ice, and  $K_I$  is the stress intensity factor at the fault tip. Normally  $K_I \propto \langle \sigma \rangle \sqrt{l}$ ; the proportionality coefficient depends on the geometry,  $\langle \sigma \rangle$  is the mean stress, and  $2l$  equals the crack length. Note that Eq. (5) is written by incorporating the correspondence principle of viscoelasticity.

In the case of the fault growing in the quasistatic regime in a viscous medium one can use the criterion of the kinetic crack theory in the following form:  $K_I = K_I^*(v)$ , where  $K_I^*(v)$  is a material function of the fault growth velocity. If the growth of an ex-

tensive initial crack starts in the quasibrittle regime, then  $K_I^* \sim K_{Ic}$ , which is the material fracture resistance in the absence of viscous effects. Then using Eqs. (5) and (6) we can write

$$x^* \sim \left( \frac{\eta v_v^x}{K_{Ic}} \right)^2 \tag{7}$$

where  $v_v^* \sim (du_v/dt)$  at  $x = x^*$  and  $x^*$  is the co-ordinate of the trailing edge of the active loaded region near the fault end. Recall that we consider an extending, growing fault such that its active loaded end region is small as compared with the fault length. More precisely, we assume that in the middle part of the fault where the velocity of the relative displacements of the fault surfaces exceeds the critical value  $v^*$ , the fault surfaces are unloaded.

For a crack in the state of the limit equilibrium under the action of the uniform load,  $\sigma$ , we can write  $K_I \sim \sigma x^*/\sqrt{l}$  and  $K_I = K_{Ic}$  where  $l$  is the fault length. To obtain a lower estimate of the value  $x^*$  in our case, we can use  $\langle \sigma \rangle$  as the characteristic stress, and thus

$$x^* \sim \frac{K_{Ic} \sqrt{l}}{\langle \sigma \rangle} \tag{8}$$

Thus the size of the active loaded end region of the growing fault should increase to provide the fault limit equilibrium.

According to Eqs. (7) and (8), the fault grows at the constant critical stress intensity factor if  $l < l^*$ , where  $l^*$  is associated with attaining the equality of the values  $x^*$  determined by these formulae,

$$l^* \sim \left( \frac{\sigma \eta^2 v^{*2}}{K_{Ic}^3} \right)^2 \tag{9}$$

Further fault growth is possible in the regime of viscous increment, accompanied by simultaneous decrease in the stress intensity factor  $K_I$  and critical stress intensity factor  $K_I^*(v)$  as the crack arrest occurs.

Let us estimate some parameters of the regime of viscous fault growth. If we assume that viscous fracture occurs at a critical level of deformation,  $\epsilon_{cr}$ , then the characteristic deformation rate in the end region of the growing crack is

$$\epsilon \sim \epsilon_{cr} \cdot \frac{v}{r} \tag{10}$$

where  $v$  is the fault velocity and  $r$  is the characteristic size of the end region ahead of the fault tip. Suppose that the characteristic deformation rate of ice can be described by

Glen's law of viscous ice flow,  $\varepsilon = B\sigma_r^n$ , where  $B$  and  $n$  are constants and  $\sigma_r$  is the critical level of stresses in the ice cover. Then we obtain

$$\sigma_r \sim \left( \frac{\varepsilon_{cr} v}{Br} \right)^{1/n} \quad (11)$$

Further, if we assume that the stresses should attain the level  $\sigma_r$  at the boundary of the fault end region, then in the state of the limit equilibrium

$$\sigma_r = K_1^* / \sqrt{2\pi r} \quad (12)$$

and according to Eqs. (11–12), the effective fracture toughness becomes

$$K_1 \sim \sqrt{2\pi} \cdot \left( \frac{\varepsilon_{cr} v}{B} \right)^{1/n} r^{\frac{1}{2} - \frac{1}{n}} \quad (13)$$

In particular, at  $n \approx 2$ ,  $K_1 \sim \sqrt{2\pi} \cdot (\varepsilon_{cr} v/B)^{1/n}$ ; the exponent value 3 as in Glen's law would result in weak dependence of  $K_1^*$  on  $r$ . Substituting the expression of  $K_1^*$  in Eq. (9), we obtain a relation between the fault velocity and its length in the regime of the fault viscous growth

$$v \sim \frac{B}{\sqrt{2\pi}\varepsilon_{cr}} \cdot \left( \frac{\sigma^2 \eta^4 v^{*4}}{l} \right)^{1/3} \quad (14)$$

Hence, as the fault length increases, its velocity decreases proportionally to  $l^{-1/3}$ .

Note that a more detailed analysis of the fault kinetics of viscoelastic thin ice can be performed on the basis of the solution of the problem on crack growth under the combined action of the wind load and the horizontal retardation reaction of the hydraulic foundation. Omitting the details, the time dependence of the fault velocity becomes

$$\frac{dl}{dt} \sim \frac{t^3 b}{(1+bt)^5} \quad (15)$$

where  $b \sim E/\eta$ . Hence the velocity initially increases and later decreases to zero. A numerical estimate for the present data show that the maximum velocity is of the order of 100 m/s, while the fault is attained at a fault length of order 3 km.

#### 4. Conclusions

We performed an analysis of remote sensing images of ice cover in the Bay of Bothnia. Characteristic structures resulting from an initially homogeneous thin-ice cover were separated. These structures can be associated with certain types of stress-deformation states of the ice cover caused by loads due to winds and sea currents.

Some problems appeared at an attempt to develop specific mechanical models of the formation of ice cover structures, and to clarify their influence on the exchange processes which connect regional and local phenomena. The main problem is associated with the insufficiency of detailed data on the geometry and time evolution, accompanying the ice cover transformations on the adjacent scales. These difficulties could be overcome by performing synchronous observations and by modelling.

At present we are completing the development of a qualitative model which describes the formation of a system of parallel faults (Table 1). The model is based on the assumption that fault growth in thin-ice cover under wind action can be arrested by hydraulic resistance. It is also essential that the main faults are oriented transverse to the wind direction. The vortex structure of ice cover (Table 1), which could be associated with the sea currents beneath the ice, needs to be studied in detail since these rotational forms of the ice motion can cause specific mechanisms of ice cover macrofracture essential for the exchange processes in the system atmosphere-ice cover-sea (ocean). In addition, the vortex structures can serve as markers of streams under the ice.

It would be desirable that field studies of localised structural elements (e.g., cracks, ridges) include: (i) observations of the geometric details of the end regions of these elements; (ii) homogeneity of the displacements in the central zones of the elements; (iii) observations of the feathering structures near the main faults; and (iv) qualitative evaluation of the displacement kinetics at the regional scale and at the scale of the characteristic structural elements.

Finally, our results from modelling the ordered fault systems can be used for solving the inverse problem in reconstructing the history of the ice cover loading. This can be attained by measuring the evolution of the fault structure parameters on the basis of a series of consecutive satellite images of the region.

#### *Acknowledgements*

This study was supported by the European Commission, DG XII, through the Marine Science and Technology Program, 1994–1998 (MAST III) under contract MAS3-CT95-0006 (ICE STATE). ICE STATE comprises Helsinki University of Technology, Nansen Environmental and Remote Sensing Center, Scott Polar Research Institute, University of Helsinki, and University of Iceland. This study was also supported by grant 96-01-00690 from the Russian Foundation for Basic Research. The ERS-1 SAR data were provided by ESA to M. Leppäranta (ERS-1 A.O project SF1). We are grateful to Tony Meadows for revision of the English language.

#### 5. *References*

- Askne, J., M. Leppäranta and T. Thompson, 1992. Bothnian Experiment in Preparation for ERS-1, 1988 (BEPERS-88) – An Overview, *International Journal of Remote Sensing*, **13(13)**, 2377–2398.

- Carlström, A. (Ed.), 1993. Baltic experiment for ERS-1. BEERS-93, Internal Report RSG 1993: 3. Department of Radio and Space Science, Chalmers University of Technology, Gothenburg.
- Goldstein, R.V. and N.M. Osipenko, 1983a. Fracture mechanics and some questions of ice fracture [in Russian], In: *Mechanika i Phisika L'da*, pp. 31–62. Moscow, Nauka.
- Goldstein, R.V. and N.M. Osipenko, 1983b. Some aspects of fracture mechanics of ice cover, *Proc. 7th International Conference on Port and Ocean Engineering under Arctic Conditions (POAC-1983)*, **3**, pp. 132–143. Helsinki.
- Goldstein, R.V. and N.M. Osipenko, 1985. Some mechanisms of localized fracture of ice cover under the action of compression, *Proc. 8th International Conference on Port and Ocean Engineering under Arctic Conditions (POAC-1985)*, **3**, pp. 1170–1188. Narssarsuaq, Greenland.
- Goldstein, R.V. and N.M. Osipenko, 1986. Ice fracture mechanics and some of its applications, *VTT Symp. 70(POLARTECH 86)*, pp. 197–210. Espoo, Finland.
- Goldstein, R.V. and N.M. Osipenko, 1987. Localized brittle fracture of thin solids with cracklike defects under compression with containment, *Mechanics of Solids (Mekhanika Tverdogo Tela)*, **22(5)**, pp. 150–159. Allerton Press.
- Goldstein, R.V. and N.M. Osipenko, 1991. Some questions on ice and ice cover fracture in compression, *Proc. IUTAM-IAHR Symp.*, St. John's, Newfoundland, pp. 251–266, Springer-Verlag, Berlin.
- Goldstein, R.V. and N.M. Osipenko, 1993. Fracture mechanics in modeling of ice-breaking capability of ship, *J. Cold Regions Eng.*, **7(2)**, 33–44.
- Hellan, K., 1986. *Introduction to Fracture Mechanics*, McGraw-Hill, N.Y., 364 p.
- Lensu, M. (Ed.), 1992. R/V Aranda base data. BEERS 92. Report 1: Ice observations and weather data, *Internal Report 1992(9)*, Finnish Inst. of Marine Research, Helsinki.
- Leppäranta, M., 1998. The Dynamics of Drift Ice, In: Leppäranta, M. (Ed.), *The Physics of Ice-Covered Seas*, **Vol. 1**, pp. 305–342. University of Helsinki Press.
- Leppäranta, M. and A. Omstedt, 1990. Dynamic coupling of sea ice and water for an ice field with free boundaries, *Tellus*, **42A**, 482–495.
- Leppäranta, M., R. Kuittinen and J. Askne, 1992. Bepers Pilot Study. An experiment with X-band synthetic aperture radar over Baltic Sea ice, *Journal of Glaciology*, **38**, 23–35.
- Leppäranta, M., M. Hallikainen, E.-A. Herland, M. Similä, R. Berglund, M. Lensu, T. Manninen and M. Toikka, 1993. Finnish ERS-1 Baltic Sea ice experiment in winter 1992, *Proc. First ERS-1 Symposium*, Cannes, France, 4–6 November 1992, pp. 307–312 (ESA SP-359).

- Riska, K., P. Kujala, R.V. Goldstein, N.M. Osipenko and V. Danilenko, 1996. Application of results from the research project “A ship in compressive ice” to ship operability, Report M-209, 16 p. Helsinki University of Technology, Ship Laboratory, Espoo.
- Ulander, L.M.H. (Ed.), 1994. Baltic experiment for ERS-1. BEERS, *Res. Report No. 51*, Department of Radio and Space Science, Chalmers University of Technology, Gothenburg.
- Zhang, Z. and M. Leppäranta, 1995. Modelling the influence of ice on sea level variations in the Baltic Sea, *Geophysica*, **31(2)**, 31–46.